TU Delft

Delft University of Technology

Document Version
Final published version

Licence
CC BY

Citation (APA)
Abdelwahab, A., Horne, F. J., Farmani, Z., Zeijl, H. V., Kuipers, H., Fan, J., & Zhang, G. Q. (2026). Contactless drop-attach adhesive bonding: An experimental study of mounting-pressure effects in microchip assembly. *Journal of Materials Research and Technology*, *43*, 2810-2824. https://doi.org/10.1016/j.jmrt.2026.06.226

Important note
To cite this publication, please use the final published version (if applicable).
Please check the document version above.

Copyright
In case the licence states “Dutch Copyright Act (Article 25fa)”, this publication was made available Green Open Access via the TU Delft Institutional Repository pursuant to Dutch Copyright Act (Article 25fa, the Taverne amendment). This provision does not affect copyright ownership.
Unless copyright is transferred by contract or statute, it remains with the copyright holder.

Sharing and reuse
Other than for strictly personal use, it is not permitted to download, forward or distribute the text or part of it, without the consent of the author(s) and/or copyright holder(s), unless the work is under an open content license such as Creative Commons.

Takedown policy
Please contact us and provide details if you believe this document breaches copyrights.
We will remove access to the work immediately and investigate your claim.

This work is downloaded from Delft University of Technology.

Journal of Materials Research and Technology 43 (2026) 2810–2824

Contents lists available at ScienceDirect

Journal of Materials Research and Technology

journal homepage: www.elsevier.com/locate/jmrt

Contactless drop-attach adhesive bonding: An experimental study of mounting-pressure effects in microchip assembly

Ahmed Abdelwahab [a,*], Fiona J. Horne [a], Zohreh Farmani [a], Henk van Zeijl [a], Hans Kuipers [b], Jiajie Fan [a], G.Q. Zhang [a]

[a] Delft University of Technology, Delft, Netherlands
[b] ITEC, Nijmegen, Netherlands

ARTICLE INFO

Keywords:
Adhesive
Bonding
die-attach
Flip-chip
Packaging
Pick-and-place
Pick-and-release
die tilt
Bond line thickness
Glue
Conductive adhesive
Shear-strength
Failure analysis

ABSTRACT

This work presents an experimental investigation of adhesive-based die attachment using the Drop-Attach technique, compared with the conventional pick-and-place method. Drop-Attach is a contactless process that eliminates the mechanical stresses inherent to force-assisted placement. In this method, dies are optically aligned and released—via a short air pulse—from a height of 100–300 μm above a substrate coated with a flat adhesive layer, enabling pressure-free, contactless placement. The process achieves smaller cycle times, potentially improving the throughput over conventional methods that require additional time for deceleration and bonding-force buildup. To assess feasibility and performance, a silver-filled bismaleimide/acrylate adhesive was printed on ENIG-finished pads, and dummy silicon dies with Au-, Ag-, and Cu-coated surfaces were assembled using both techniques. Bond quality was comprehensively analysed through measurements of bond line thickness, die tilt, void formation, die-shear strength, failure mechanisms, and electrical performance. Drop-Attach achieved minimal die tilt ($\leq 0.1°$) and uniform BLTs, though higher voiding and ~9.55% increased electrical resistance were observed. The lower shear strength was primarily attributed to the absence of adhesive fillet formation rather than the lack of applied pressure. While trade-offs remain, this study demonstrates the feasibility of adhesive-based die attachment using the Drop-Attach method, which enables faster cycle times and higher throughput while significantly reducing mechanical stresses. These advantages position Drop-Attach as a promising technique for next-generation semiconductor packaging.

1. Introduction

Adhesive bonding has emerged as a fundamental technology in the electronics and semiconductor fields, with more than 50,000 conductive and non-conductive adhesive formulations in global use today [1]. Silver-filled conductive adhesives represent the largest category of thermal die-attach materials used in semiconductor packaging, extending beyond LED applications [2]. Its applications are widespread, particularly in packaging for microelectronics and the rapidly growing power electronics sector [1,3]. Its versatility enables cost-effective, low-temperature, and environmentally friendly alternatives to conventional interconnect technologies such as soldering—especially in high-density, miniaturized electronic assemblies. Among the various classes of adhesives, Non-Conductive Adhesives (NCAs)— and Electrically Conductive Adhesives (ECAs)—including Isotropic Conductive Adhesives (ICAs), Anisotropic Conductive Adhesives (ACAs), are increasingly deployed in fine-pitch interconnects and advanced packaging configurations. ICAs serve as effective solder replacements in surface-mount and flip-chip applications, while ACAs—particularly in film form (Anisotropic Conductive Films, or ACFs)—have been widely adopted in flat panel display modules for their excellent performance in lightweight, thin, and low-power electronic systems [1,3–7]. These materials not only provide mechanical bonding but also enable electrical interconnection through the incorporation of conductive fillers within a polymer matrix, making them indispensable when process limitations such as temperature, substrate compatibility, or pad pitch prevent the use of traditional soldering [1,7–9].

Conventional die bonding techniques rely heavily on mechanical force to mount semiconductor dies onto substrates, typically applying bonding forces in the range of 0.2–1 N [10]. However, as chips become

* Corresponding author.
E-mail addresses: a.n.m.k.abdelwahab@tudleft.nl (A. Abdelwahab), f.j.horne@tudelft.nl (F.J. Horne), zfarmani@tudelft.nl (Z. Farmani), H.W.vanZeijl@tudelft.nl (H. Zeijl), j.j.kuipers@itecequipment.com (H. Kuipers), J.Fan-3@tudelft.nl (J. Fan), G.Q.Zhang@tudelft.nl (G.Q. Zhang).

https://doi.org/10.1016/j.jmrt.2026.06.226
Received 11 December 2025; Received in revised form 15 June 2026; Accepted 23 June 2026
Available online 24 June 2026
2238-7854/© 2026 The Authors. Published by Elsevier B.V. This is an open access article under the CC BY license (http://creativecommons.org/licenses/by/4.0/).

increasingly thinner to meet the demand for vertically stacked and compact package architectures, their mechanical fragility also increases [11–14]. Additionally dies with fragile components such as thin membranes are susceptible to damage during the bonding process [15,16]. The mechanical and thermal stresses introduced during pick-and-place operations—particularly during die landing—pose significant risks of die cracking and long-term reliability issues [17,18]. Even with carefully controlled landing speeds and deceleration profiles, the need for precise alignment and stress mitigation continues to constrain throughput and yield in standard die attach processes.

To address these challenges, this study explores the potential of adhesive bonding within a novel contact-less die attach process based on pick-and-release [19]. In this approach, dies are optically aligned and released in close proximity to the substrate without direct contact or applied pressure—thereby eliminating the mechanical stress typically induced during conventional pick-and-place operations. This mechanism achieves release travel speeds of up to 125 μm/ms and release times as short as 1 ms. This high speed significantly increases throughput while still preserving die integrity [10]. This high-speed, contactless process is especially suitable for handling ultra-thin and delicate components, offering promising potential for laser die transfer (LDT) applications, where achieving bonding without applied pressure is crucial.

Within the framework of the proposed die drop technique, maintaining a flat and uniform adhesive surface is critical to ensure accurate die placement and to reduce tilt, even in the absence of external bonding force. Conventional dispensing techniques may not meet the necessary surface uniformity requirements for contact-less die attach. Therefore, stencil printing is utilized to apply adhesive over relatively large areas, yielding smooth and consistent layers that facilitate precise, pressure-less die placement. Through a detailed evaluation of adhesive performance under these new process conditions, this work aims to highlight the pivotal role of the drop-attach method with adhesives in enabling next-generation semiconductor packaging technologies.

2. Drop-attach method

In the conventional Pick-and-Place method shown in Fig. 1(a), an electronic component is first positioned and aligned above its target location and then pressed downward onto the bonding material or carrier with a controlled force before release. This minimal yet precise force helps flatten the bonding material layer [20–22]. While effective, this approach inherently introduces mechanical stress and increases the risk of damaging fragile components of the chips. In contrast, the Drop-Attach method shown in Fig. 1(b) maintains a consistent alignment height while completely eliminating direct contact with the adhesive or substrate during component placement. In this approach, the component is gently released from a short distance above the target site, allowing it to descend accurately under the effect of gravity, thereby achieving a contact-free, low-stress bonding process. Specifically, in our experiments, dies were picked up using a vacuum gripper and subsequently released through a brief, controlled air pulse lasting 10-100 ms at a pressure of 0.1-0.15 bar. The proposed technique substantially accelerates the assembly process by eliminating the need for die deceleration prior to touchdown. In conventional approaches, dies must reduce their velocity to prevent mechanical damage caused by the relatively high-speed impact with the substrate. In contrast, the proposed method allows the dies to be released from a relatively large distance above the substrate, thereby removing the requirement for a controlled approach phase. As no physical contact occurs during release, the dies can maintain their full operational velocity without risk of unintended impact or collision.

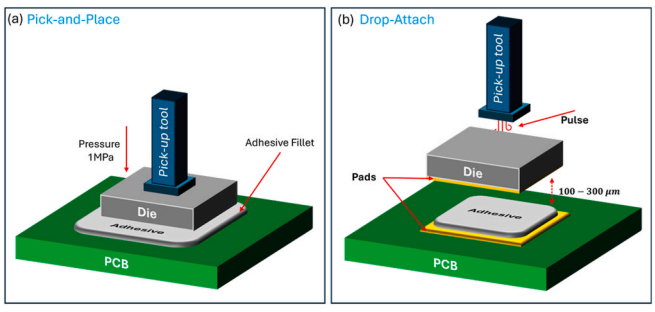


Fig. 1. Sketch of the die attach processes studied in this work. (a) Traditional pick-and-place, (b) the proposed Drop- Attach.

3. Experimental

3.1. Bonding material and stencil printing

A commercially available conductive adhesive was selected for the die-attach process. The formulation contains approximately 80% silver by weight, dispersed within a polymeric acrylate-based resin matrix that cures to form the structural binder. The adhesive is processed using a snap-cure profile requiring 60 s at 185 °C on a hot plate.

A 100 μm-thick laser-cut stainless-steel stencil was used with a manual eC-stencil-mate (Eurocircuits) to transfer adhesive deposits to the metal pads patterned on the substrate.

The printed adhesive pattern displayed noticeable imperfections, particularly at the edges, characterized primarily by increased adhesive thickness. This edge thickening is likely attributed to the separation process of the stencil mask from the substrate, during which residual adhesion between the adhesive and the stencil mask causes deformation or distortion. Such defects can be eliminated by optimizing the printing process or by using advanced automated stencil printers. In conventional die attach processes, such slight irregularities are typically not problematic, as the application of even a small bonding force helps to level the adhesive and ensure good contact between the die and the substrate. In contrast, in the proposed contactless method, the die is released from a short distance and lands on the adhesive under its own weight, without any applied force. Due to the die's low mass and lack of external pressure, it was observed that it cannot level out surface non-uniformities, which can result in poor adhesion and die tilt. To address this, the substrate design was modified so that the metal pads are slightly larger than the die dimensions. This ensures a more uniform adhesive distribution in the central region of the pads, enhancing alignment and bonding quality for the contactless attachment process. However, in cases where an automatic stencil printer or Laser Induced Forward Transfer (LIFT) technique is used, such precautions are less critical, as these methods can provide a well-defined geometry of the bonding material.

3.2. Substrate and dies fabrication

A printed circuit board (PCB) was designed with arrays of bond pads having dimensions slightly larger than the corresponding die sizes to ensure a flat and uniform adhesive layer over an area at least equal to the die footprint. The pads dimensions were designed to be larger by approximately 7.5–15% relative to the die sizes. For instance, a 1 × 1 mm die was matched with 1.15 × 1.15 mm pads, while the largest die, measuring 4 × 4 mm, was paired with 4.3 × 4.3 mm pads. The PCBs were fabricated with an electroless nickel immersion gold (ENIG) surface finish to ensure corrosion resistance, reliable electrical connectivity, and compatibility with the used conductive adhesive. ENIG provides a smooth, oxidation-resistant surface that supports consistent adhesive deposition and maintains stable electrical contact over time, making it a widely used finish for die attach in microelectronics. [23–25]. Fig. 2(a) shows the PCB design and Fig. 2(b) shows the PCB cross-section.

Dummy dies with different surface finishes were fabricated using 4-inch, single-side-polished silicon wafers (525 μm thick). First, a 300 nm

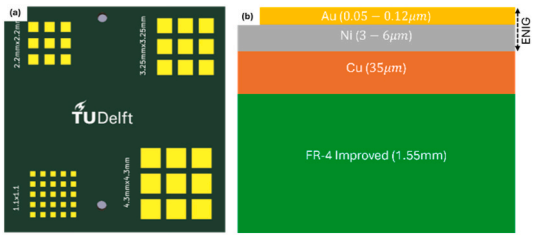


Fig. 2. (a) PCB design, (b) sketch of the PCB cross-section (not to scale).

SiO_2 layer was grown on all wafers through wet oxidation. For the gold (Au) finish, a 10 nm chromium (Cr) adhesion layer was evaporated, followed by a 200 nm Au layer. Similarly, for the silver (Ag) finish, a 10 nm titanium (Ti) adhesion layer was deposited by evaporation, followed by evaporation of a 200 nm Ag layer. The copper (Cu) finish employed a different deposition method: a 200 nm Ti layer was sputtered as both an adhesion layer and diffusion barrier, followed by a 200 nm sputtered Cu layer. Fig. 3 shows cross-sectional sketch of the different dummy dies. Following the fabrication process outlined earlier, all wafers were diced to the required dimensions by saw dicing (Disco DAD321, S2040 dicing blade).

3.3. Die attachment

The experiments were conducted using a Tresky T-3000-PRO semi-automatic die bonder. In the air-drop tests, dies were picked up with a vacuum gripper, optically aligned near the substrate, and released from a height of 100–300 μm above the adhesive layer deposited on the substrate. The release was tiggered by an air pulse of 0.15 bar applied for 100 ms. Theoretical estimation of the die free-fall velocity when assuming negligible air resistance, was calculated to be 44.3 μm/ms for a fall height of 100 μm and 76.7 μm/ms for a fall height of 300 μm.

To precisely measure the die velocity experimentally, a high-speed camera (FASTCAM Nova S16) mounted on the test setup recorded the release process from a 300 μm height above the adhesive layer at a frame rate of 9000 FPS. Analysis of the footage showed an average die velocity of 107 μm/ms. This higher value, compared to the theoretical free-fall speed, was attributed to the additional force applied by the compressed air pulse during release. Fig. 4 show a schematic of the experimental setup used for the die attach process and Fig. 5 shows the release process.

Reference samples were assembled using a standard pick-and-place process, applying a mounting pressure of 1 MPa. As the adhesive layer was flat, this pressure was sufficient to squeeze a portion of it beyond the die edges, forming a fillet around the die. This ensured uniform contact and proper interface formation, which is expected to influence the bond strength. This experimental framework enabled direct comparison between pick-and-place and drop-attach techniques, highlighting their respective impacts on adhesive behaviour, placement accuracy, and bond formation.

To provide additional insight into the dynamics of the drop-attach process, transient 3D multibody simulations were performed for a 2 mm × 2 mm × 0.5 mm silicon die released from heights of 300 μ m and

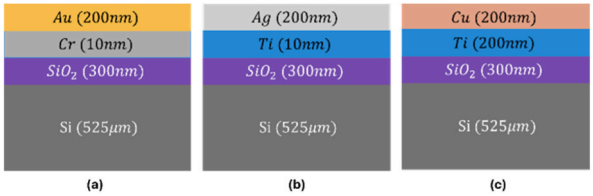


Fig. 3. Cross-sectional sketch (not to scale) showing layers stacking of the dummy dies with different surface finish (a) Gold, (b) Silver, and (c) Copper.

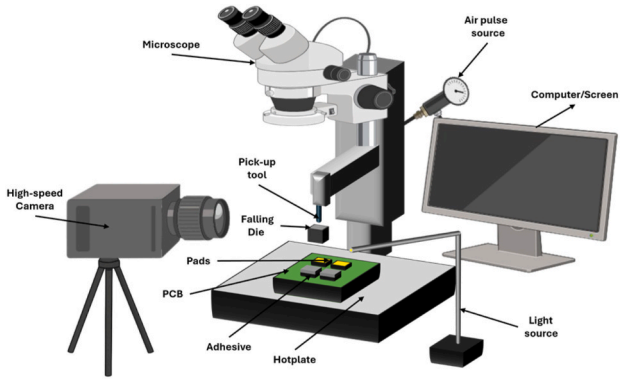


Fig. 4. Schematic of the experimental setup showing the die bonder equipped with a high-speed camera.

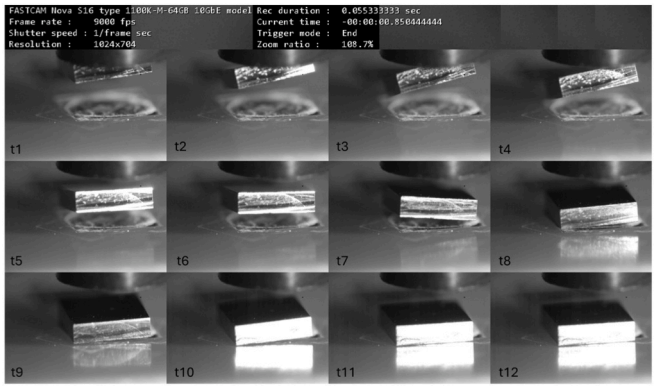


Fig. 5. Snapshots from high-speed camera footage showing die release process using Tresky T-3000-PRO die bonder.

1000 μ m above a rigid substrate, together with a conventional bonding case in which a nominal pressure of 1 MPa was applied through a 1 mm diameter loading area. In the absence of an adhesive layer, the simulated impact velocity for the 300 μ m release height was approximately 0.065 m/s, corresponding to a kinetic energy of approximately 1×10^{-8} J. Following first contact, the die reached zero vertical velocity after approximately 7 ms, with a stopping distance of approximately 0.24 mm. The simulations further showed that rebound behaviour strongly depends on release height, with rebounds observed for the 1000 μ m case, whereas negligible rebound occurred for the 300 μ m case.

Fig. 6 compares the pressure distributions obtained for the three loading scenarios. The drop-attach process generated pressure levels in the order of pascals to tens of pascals, whereas the bonding-force case produced pressures approaching 7×10^5 Pa. These results indicate that the mechanical loading associated with drop attachment is several orders of magnitude lower than that generated by conventional force-assisted bonding.

Although the adhesive layer was not explicitly included in the model, its role in dissipating impact energy can be estimated using a Kelvin–Voigt viscoelastic model consisting of a spring and dashpot acting in parallel. Under this approximation, the viscous energy dissipation scales as $E_{visc} \sim \eta(A/h)v^2t_s$ [26] where (η) is the adhesive viscosity, (A) is the die area, (h) is the adhesive thickness, (v) is the impact velocity, and (t_s) is the stopping time. Using the experimentally measured adhesive thickness of approximately 91 μ m for the 2.2 mm × 2.2 mm pad, the viscosity required to dissipate the entire die kinetic energy is estimated to be on the order of 10^{-2} Pa·s. This value is several orders of magnitude lower than the viscosity of the adhesive used in this study ($\eta = 18.5$ Pa·s), suggesting that viscous dissipation within the adhesive is sufficient to absorb a substantial fraction of the impact energy.

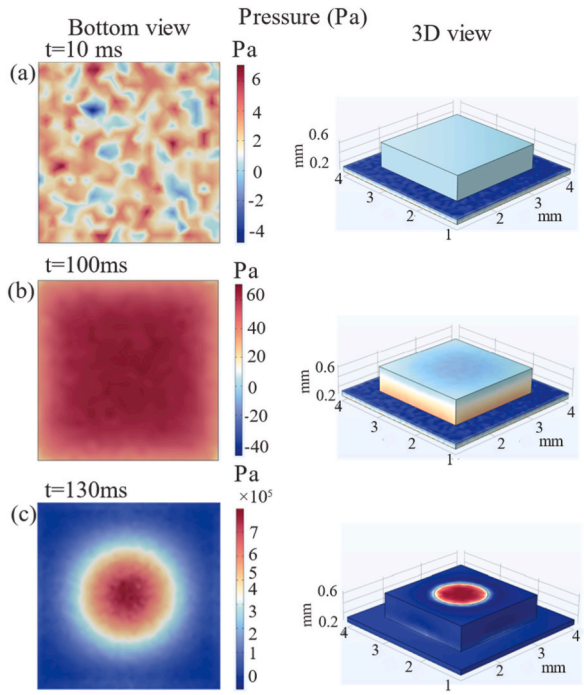


Fig. 6. Comparison of pressure distributions obtained from transient 3D multibody simulations for (a) drop attachment from a release height of 300 μm, (b) drop attachment from a release height of 1000 μm, and (c) conventional bonding with a nominal pressure of1 MPa applied through a 1 mm diameter loading area.

This observation is consistent with the experimentally observed limited reduction in bond-line thickness after drop attachment, in contrast to the pronounced adhesive spreading and fillet formation observed under a mounting pressure of 1 MPa. Nevertheless, a rigorous determination of peak adhesive pressure, strain rate, and individual dissipation pathways would require coupled die–adhesive simulations and dedicated high-speed displacement or force measurements, which are beyond the scope of the present study.

To evaluate potential throughput improvements, an industrial-scale automatic die bonder was employed. In these experiments, dies were attached using both the conventional method and the drop-attach method.

During die attachment, a high-speed camera (Phantom V711) was used to record the process. The dies were commercially available, with dimensions of 250 μm × 250 μm × 140 μm. The adhesive was deposited using the integrated dispensing system of the die bonder. A flat line of adhesive was printed directly onto a copper substrate (lead frame), with a controlled thickness of approximately 20 μm.

The analysis combined high-speed footage with machine parameters, including the collet travel speed before touchdown (25 μm/ms) and the bond force build-up time (15 ms). The machine was operated at 60,000 UPH, corresponding to 60 ms per die under conventional conditions.

In the drop-attach method, the bond force build-up time is completely eliminated. Additionally, the final 100 μm approach distance, which takes 4 ms at 25 μm/ms in the conventional process, is reduced to 0.8 ms due to the higher travel velocity (~125 μm/ms) observed from high-speed imaging.

Overall, the drop-attach method reduces the cycle time per die by approximately 18.2 ms, corresponding to an estimated time cycle reduction by ~30.33%.

It should be noted that the estimated throughput of ~86,000 UPH represents a theoretical maximum based on the reduced cycle time and was not achieved experimentally. The die bonder is rated for a maximum throughput of 60,000 UPH, and continuous operation beyond this limit was avoided to prevent potential damage or accelerated wear in the mechanical and electrical subsystems, particularly in high-speed moving components. In addition, the vacuum pick-up and release cycles are inherently limited by the machine design and were not optimized for higher-throughput operation. Therefore, the experiments were limited to 900 cycles per test to ensure safe and reliable operation.

Fig. 7 shows the automatic die bonder setup while Fig. 8 presents snapshots of the die release process. Fig. 9 shows a 3D scan of multiple 250 μm × 250 μm dies dies assembled using the automatic die bonder via the drop-attach method.

4. Materials and geometrical characterization

4.1. Material analysis

The adhesive was characterized at different stages of the process: as a freshly printed wet paste and after final curing. Inspections were carried out using Phenom XL G2 desktop scanning electron microscope (SEM) equipped with energy-dispersive X-ray spectroscopy (EDS), as well as an optical microscope. This approach enabled the evaluation of morphological changes and potential void formation associated with the decomposition or evaporation of volatile components during drying and curing. Additionally, surface roughness measurements were performed using a 3D laser scanning microscope (Keyence VK-250) and its dedicated analysis software. SEM analysis revealed a small fraction of microvoids, which are not expected to compromise the overall bond quality. However, identifying such defects prior to the bonding process is essential to distinguish between intrinsic material defects and those introduced during the bonding process. The surface roughness (Sa) derived from 3D scans over a 4.3 mm × 4.3 mm region was 2.334 μm before curing and 3.031 μm post-curing. Fig. 10(a) shows EDS mapping of the adhesive before curing and Fig. 10(b) shows EDS mapping of the adhesive after curing, where some micro voids were detected (marked in red).

4.2. Adhesive volume and profile

To assess potential manual stencil printing defects and curing-induced effects such as shrinkage or voids formation, some experiments were conducted with no dies attached. A key focus of these tests was measuring the volume and the average thickness of the printed adhesive and to ensure that the manual stencil printing process yielded a flat and uniform print profile. Upon inspection, few PCBs were rejected due to irregularities in the printed adhesive profile, particularly the formation of high peaks of adhesive at the pad edges, rendering them unsuitable for the proposed drop-attach method. The measured average adhesive thickness is presented in Table 1.

Although the adhesive is specified to cure at 180 °C for 60 s, there was concern that rapid heating could induce imperfections, such as trapped volatiles or uneven shrinkage. To address this, the curing step was conducted separately and the cured adhesive was inspected. Our verification showed that when the recommended curing profile was followed, the adhesive layer cured smoothly and uniformly, with no optically visible large defects. This outcome was achieved under the condition that the print profile exhibited uniform flatness, which ensured optimal adhesive performance and preserved the integrity of the deposited layer. The adhesive volume was measured before and after curing for each pad size using a 3D confocal laser scanning microscope. In addition to volume measurements, the average adhesive layer thickness was extracted from the 3D scans. A theoretical volume was calculated by assuming a uniform, flat adhesive layer fully covering the entire pad area—modelled as a thin film or rectangular cuboid. When comparing this theoretical volume to the actual volume obtained from the 3D scans, the printed adhesive consistently exhibited a smaller volume regardless the aperture size. This discrepancy was most apparent for the 1.1 mm × 1.1 mm pads, where the deposited adhesive adopted a

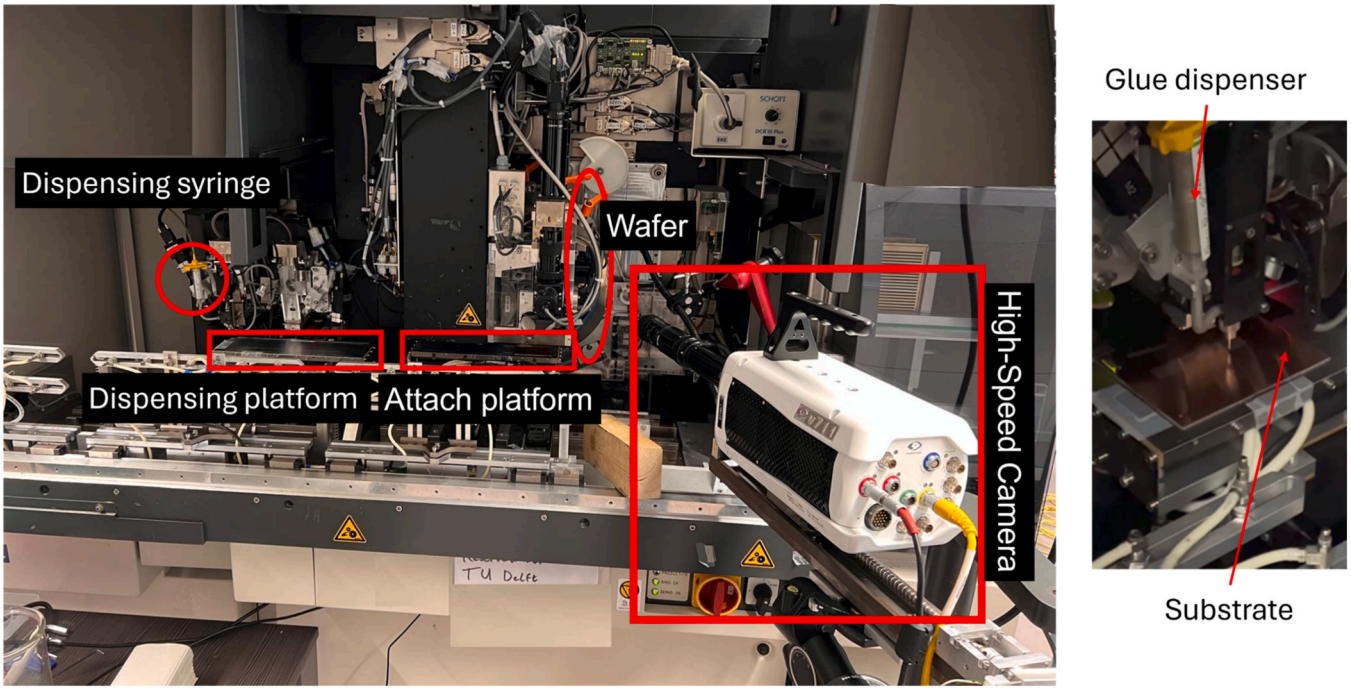


Fig. 7. Experimental setup featuring an automatic die bonder integrated with a precision dispensing unit and a high-speed imaging system for dynamic process characterization.

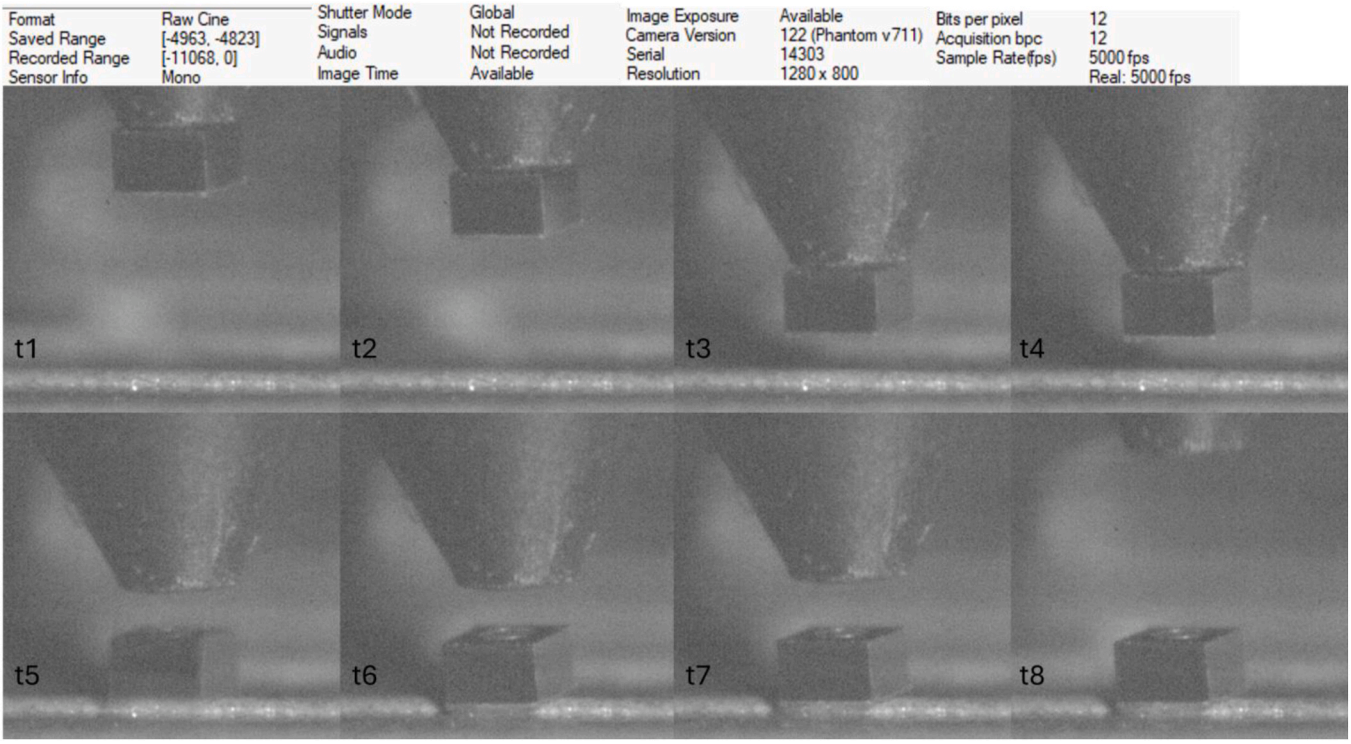


Fig. 8. High-speed camera footage recorder for a 250x250 μm die released using automatic die bonder on a flat adhesive line.

more rounded profile rather than a uniform flat square layer, primarily due to the characteristics of the printing method. Nevertheless, because the pads and stencil apertures were designed to be 10% larger than the die size, the adhesive deposition still provided a flat and uniform printed area of at least 1 mm^2 at the centre, which was considered suitable for the proposed drop-attach method. Such defects were important to analyse, solve and isolate before proceeding with the assembly. Fig. 11 shows the observed print defect for the 1.1mmx1.1 mm aperture. The measured pre-cure and post-cure volumes are summarized in Table 2.

A consistent reduction in volume post-curing was observed across all pad sizes, attributed to adhesive shrinkage during the curing process. The extent of shrinkage varied depending on the pad size, with the lowest reduction observed for the 2.2 mm × 2.2 mm pad size (21.25%) and the highest for the 3.25 mm × 3.25 mm pad size (25.42%).

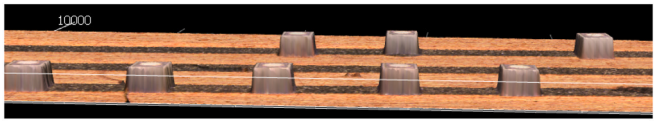


Fig. 9. Three-dimensional view reconstructed from confocal microscope scans of dies assembled using the automatic die bonder, showing multiple dies attached along a continuous adhesive flatline.

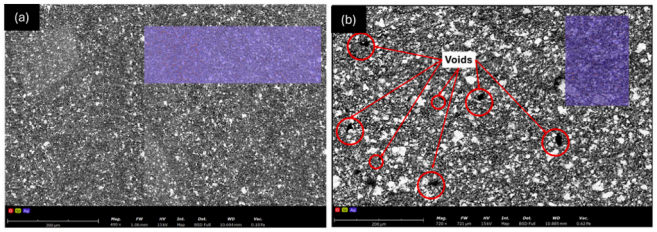


Fig. 10. SEM/EDS mapping of the printed adhesive (a) before curing (b) after curing showing few defects/micro voids.

Table 1
Adhesive composition.

Material	Weight %	Primary Role
Silver metal	>80	Conductive network (electrical and thermal)
Isobornyl methacrylate	<10	organic resin matrix, curable binder
Amines, C36-alkylenedi-, maleated	<5	Curing agent
2-(3,4-Epoxycyclohexyl) ethyltrimethoxysilane	<1	Adhesion promoter
2-Propenoic acid, 2-methyl, palladium (2+) salt	<1	Catalyst

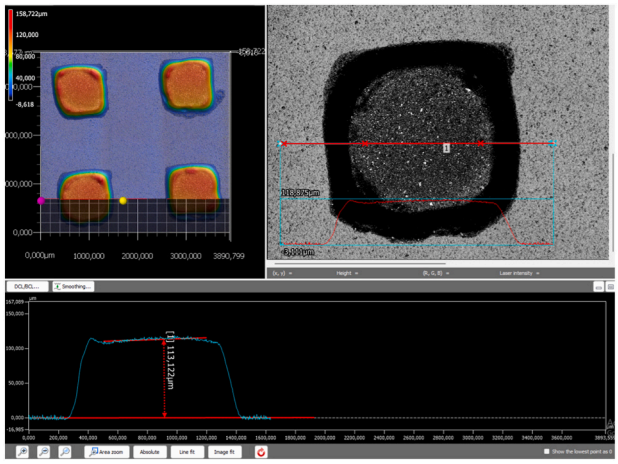


Fig. 11. 3D-scan adhesive printed on an area of 1.1 mm × 1.1 mm showing a more rounded shape differing from the square stencil apertures design.

Figs. 12 and 13 showing example of the adhesive thickness printed on area of 4.3mmx4.3 mm before and after curing respectively.

4.3. Bond line thickness and die tilt

The bond line thickness (BLT) is a key parameter influencing the mechanical reliability, electrical performance, and thermal resistance of an interconnect. Given its critical role, an accurate measurement of the BLT was essential [27].

Table 2
Average adhesive layer thickness before and after curing for different pad sizes.

Pad size (*mm*)	adhesive thickness before curing (μm)	Adhesive thickness after curing (μm)
1.10x1.10	110.06 ±2.34	83.51 ±2.33
2.20x2.20	90.97 ±1.74	65.15 ±1.56
3.25x3.25	89.22 ±1.66	63.74 ±1.81
4.30x4.30	87.29 ±2.20	63.54 ±2.13

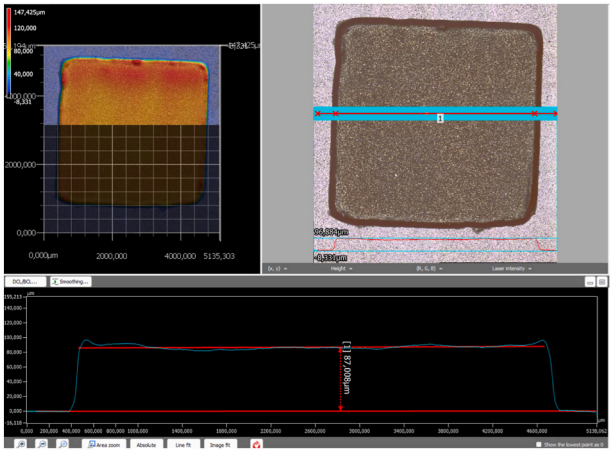


Fig. 12. Profile of printed adhesive on an area of 4.3 mm × 4.3 mm before curing showing the adhesive thickness of 87 μm.

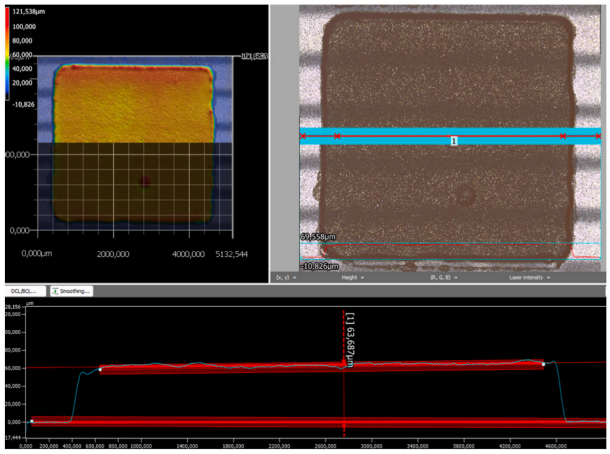


Fig. 13. Profile of printed adhesive on an area of 4.3 mm × 4.3 mm after curing showing the adhesive thickness reduced to 63.69 μm.

3D laser scans were employed to obtain high-resolution surface profiles for estimating the bond line thickness (BLT) by measuring the height difference between the die and the PCB pad surface. A more complex, indirect method was initially considered to account for potential die tilt and provide a more accurate BLT estimation [27]. This approach relied on comparing die corner heights to reference points on the PCB. However, post-assembly inspection revealed that only a few dies exhibited noticeable tilt ($\geq 2^{\circ}$). Consequently, these samples with higher tilt were excluded from the study, and the simplified direct measurement method was applied to the remaining population. The observed tilt was attributed to misalignment during the die drop process, causing some dies to land near the edges of the adhesive pattern, where the adhesive thickness was slightly higher than in the more uniform central region. Although the 1.1mmx1.1 mm aperture yielded a flat area

of at least $1mm^2$ but with some defects as shown in Fig. 11, it was essential to validate that such defects didn't have any negative influence on the assembly, some reference samples of the 1mmx1mm dies were attached on an adhesive layer but printed on a larger pad with no visible defects. These reference samples showed no difference to the original samples, therefore the original assembly was considered defect free. Fig. 14 shows the 1mmx1mm reference dies attached on a 4.3mmx4.3 mm pad.

All dies examined in this study showed low die tilt ($\leq 0.1°$) on both X and Y axes. Fig. 15 shows an example of measuring die tilt of a 4mmx4mm showing a die tilt of only 0.064°. In addition, no variance in BLT across the different surfaces finishes was observed for the same die size. The BLT varied by die/pad size as a direct result of the variance observed in adhesive thickness manually printed.

The average adhesive layer thickness was measured prior to die attachment, and for dies attached without any pressure or force applied, the BLT was expected -under the condition of zero force application-to match the adhesive thickness exactly. However, a slight reduction in BLT was observed after the dies were dropped, indicating that the adhesive layer underwent minor compression or lateral spreading as a result of the die impact. This effect can be conceptually translated into a pressure applied by the die onto the adhesive layer. However, to accurately quantify such pressure, additional parameters such as the exact stopping distance and stopping time would be required, which were not measured in this study. Instead, the kinetic energy of the die prior to impact was determined as a first-order measure of the mechanical load associated with the drop event. The kinetic energy of a 2mmx2mm die was calculated using the following equation $E_k = \frac{1}{2}mv^2 \approx 2.8 \times 10^{-8} J$ [28]. Additionally, the BLT decreased after the curing step, which can be attributed to the reduction in adhesive volume during the curing process which was measured and recorded before the assembly process. A similar pattern was observed for the dies attached with 1 MPa of mounting force. In this case, the BLT was noticeably lower than the printed adhesive thickness, which can be directly attributed to the applied pressure. The pressure compressed the adhesive material and caused it to spread outside the borders of the pads, creating a fillet shape, as shown in Fig. 16(a) while in Fig. 16(b) no presence of such adhesive fillet observed for dies attached with the drop-attach method. In Tables 3 and 4, a summary of the BLT measurements is presented, highlighting the changes observed before and after die attachment, as well as after the curing process.

From the BLT measurements, it can be concluded that on average the BLT of the dies attached without pressure shrunk by 37.9% after curing, while the dies attached with pressure showed an average shrinkage of 33.77%. The main difference observed is the BLT directly after die attach and before the curing step. Since no external pressure was applied during the pressure-less attach process, the adhesive layer was mainly deformed by the impact of the die, which may have limited the spreading of the adhesive. As a result, only a relatively small variation in BLT was observed, likely due to the limited die mass and impact velocity. During the curing process, both attachment methods showed a similar reduction in BLT, indicating that the adhesive exhibited comparable curing behaviour regardless of whether pressure was applied during die attach.

The observed differences in bond-line thickness and fillet formation can be interpreted in terms of adhesive flow and wetting dynamics. During die placement, the adhesive undergoes a transient squeeze-flow process [29,30] in which the adhesive is confined and displaced within a progressively decreasing gap and is forced to flow radially outward. The extent of this flow depends on the balance between the applied load, the

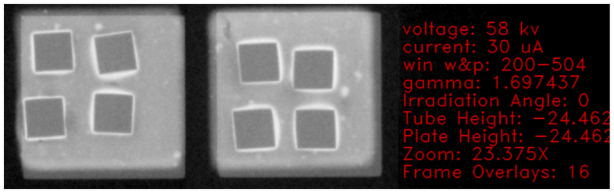


Fig. 14. X-Ray image of 1mmx1mm dies attached on adhesive layer printed over 4.3mmx4.3 mm bond pad.

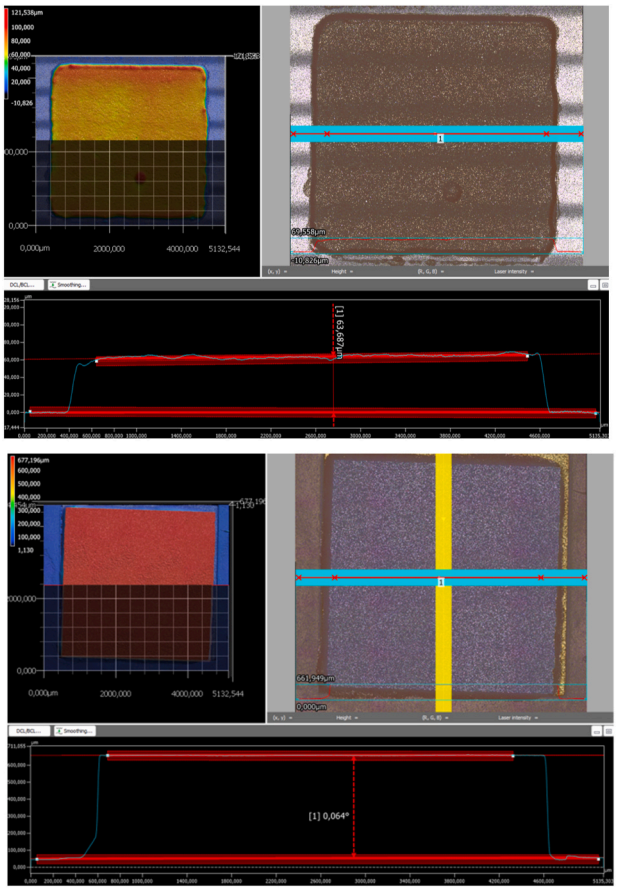


Fig. 15. 3D-scan of a 4 mm × 4 mm die attached via drop-on method, revealing minimal tilt (0.064°) post-curing.

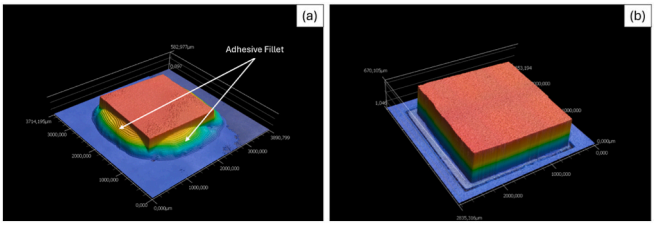


Fig. 16. 3D surface scans of dies attached to adhesive layers under different bonding conditions: **(a)** Die mounted at 1 MPa pressure, showing characteristic adhesive fillet formation due to squeeze-out beneath the die edges; **(b)** Die attached via drop-on method, demonstrating absence of fillet formation.

Table 3
Adhesive volume before and after curing for different pad sizes.

Pad size (mm)	Theoretical printed volume (μL)	Volume as printed (μL)	Volume after curing (μL)	Actual reduction %
1.10x1.10	0.1338	0.1011	0.078	22.87
2.20x2.20	0.4403	0.3842	0.3026	21.25
3.25x3.25	0.9424	0.8477	0.6322	25.42
4.30x4.30	1.6103	1.5652	1.2001	23.33

Table 4
Estimated BLT of dies attached by Drop-attach method.

Die Size (mm^2)	Adhesive thickness (μm)	Estimated BLT after die attach (μm)	Estimated BLT after curing (μm)
1x1	110.06 ± 2.34	99.07 ± 2.04	64.88 ± 2.03
2x2	90.97 ± 1.74	87.48 ± 1.54	54.16 ± 3.33
3x3	89.22 ± 1.66	85.10 ± 1.47	53.23 ± 4.88
4x4	87.09 ± 2.20	85.68 ± 1.91	50.11 ± 5.91

Table 5
Estimated BLT of dies attached by pick-and-place method.

Die Size (mm)	Adhesive thickness (μm)	Estimated BLT after die attach (μm)	Estimated BLT after curing (μm)
1x1	110.06 ±2.34	52 ± 5.05	29 ± 5.11
2x2	90.97 ±1.74	46 ± 2.22	31 ± 2.33
3x3	89.22 ±1.66	49 ± 4.81	33 ± 4.50
4x4	87.09 ±2.20	43 ± 4.12	32 ± 4.66

viscous resistance of the adhesive, and wetting at the die–adhesive and substrate–adhesive interfaces. For a viscous adhesive layer, the characteristic squeeze-flow resistance scales as $\left(F_{\{squeeze\}} \propto \eta\ Vh^{-3}\right)$, where η is the adhesive viscosity, V is the approach velocity, and h is the adhesive thickness. Using the measured adhesive viscosity ($\eta = 18.5$ Pa·s), an initial adhesive thickness of approximately 91 μ m, and the simulated impact velocity of 0.065 m/s, the resulting squeeze-flow resistance is estimated to be on the order of 10^{-2} N. This value is substantially larger than the die weight, indicating that viscous resistance can strongly damp the die motion and limit rapid adhesive redistribution during impact.

For the drop-attach process, the die impacts the adhesive with relatively low kinetic energy ($\sim 10^{-8}$ J), resulting in only limited compression of the adhesive layer. Therefore, the adhesive remains largely confined within the original stencil-printed footprint and no significant fillet formation is observed. This indicates that the advancing contact line undergoes only limited displacement during attachment, suggesting that the wetting process is dominated by local interface formation rather than extensive radial flow of adhesive. Consistent with this interpretation, only a minor reduction in bond-line thickness is measured after die placement. As wetting proceeds, new die-adhesive and substrate-adhesive interfaces are created, requiring advancement of the contact line. The limited adhesive flow observed during drop attachment therefore restricts contact-line propagation and adhesive spreading compared with the pressure-assisted case.

In contrast, when a mounting pressure of 1 MPa is applied, the adhesive experiences sustained compressive loading, generating pressure-driven squeeze flow [31] within the bond line. The resulting radial transport of adhesive causes the contact line to advance beyond the pad boundaries, producing the fillet structures observed in Fig. 16(a). The larger reduction in bond-line thickness measured in this case is therefore attributed to enhanced adhesive redistribution rather than solely to elastic compression of the adhesive layer.

These observations indicate that the differences between drop attachment and conventional bonding arise from the distinct squeeze-flow and wetting dynamics governing adhesive redistribution during attachment.

5. Results

5.1. X-ray inspection

X-ray imaging was conducted using a SEAMARK X5600 offline X-ray inspection system to evaluate the quality of die attachment. The inspection aimed to assess the interfacial contact between the dies and the adhesive, as well as to identify voids and interfacial discontinuities. Since no external pressure was applied during assembly, limited wetting and partial contact were expected, potentially representing the weakest point of the joint. Image analysis was performed using ImageJ software to quantify the contact area as a percentage of the total die area, providing a measure of adhesive coverage.

The void area observed for each die size is summarized in Table 5, comparing samples attached using the drop-attach method with those mounted by a conventional method applying 1 MPa pressure. Dies attached via the drop-attach method exhibited a higher number of voids than those attached conventionally. Three distinct defect types were identified: micro-voids, larger voids, and edge defects. Representative X-ray images highlighting these voids are presented in Figs. 17 and 18. In particular, the occurrence of large voids in the central region of dies assembled without pressure. However, the origin and mechanism behind the formation of the large central voids required further investigations, some discussed in section D. The first explanation to such findings is based on the initial contact geometry where the die firstly made contact with the slightly higher edges of the printed adhesive, sealing the edges before the centre of the die has made contact with the adhesive. This creates a closed boundary that traps the air in the centre (see Table 6).

Table 6
Defects and void area for each die size derived from X-ray imaging.

Die size (mm)	Void area	
	Drop-attach	1 MPa pressure
1.x1	Almost no voids with some edge defects	Few micro voids in the centre area for all dies
2.x2	Voids area ≤ 3% with some edge defects	Almost no voids, with few micro voids along the edges in case of Au dies only
3x3	Larger voids with area ≤ 10%	Voids area ≤ 1%
4x4	Larger voids with area ≤ 7%	Voids area ≤ 2%

To validate such assumption a control samples were created, in such samples the dies were dropped on a relatively larger print area, in this approach the focus was on creating a big enough landing site with no defects. For instance the observed defect associated with the 4mmx4mm was tested again on much larger adhesive pattern of around 20mmx20mm. The patterns were created by a simple mask made by laser cutting Kapton film. It was observed that such defects where eliminated. An x-ray image showing the dropped dies on the new pattern in Fig. 19(b).

These findings indicate that the footprint of the dies has a direct influence on void formation. Larger footprints, such as in full-die attachments, exhibited more pronounced voiding, whereas dies with smaller footprints (up to 1 mm × 1 mm) showed almost no voids. Despite the presence of such defects, the maximum void area detected across all samples remained ≤10%. This suggests that in industrial applications, where dies are divided into multiple smaller pads or Inputs/Outputs (I/

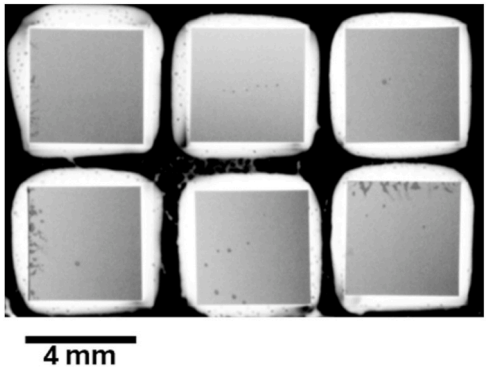


Fig. 17. X-Ray of 4mmx4mm Au dies attached with 1 MPa showing some micro voids in the centre of the dies and some defects along the edges of the die.

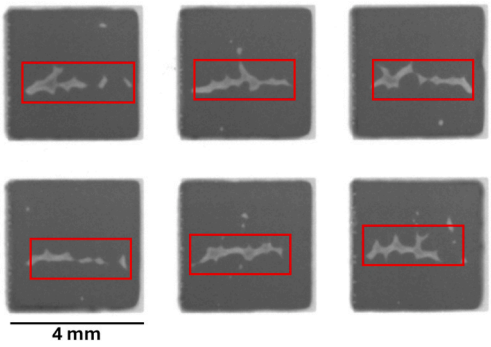


Fig. 18. X-Ray of 4mmx4mm Au dies attached without pressure showing large voids in the centre of the dies marked in red.

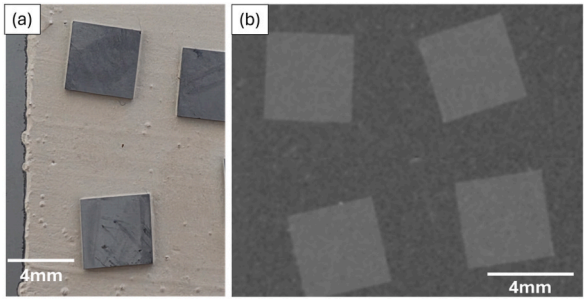


Fig. 19. Image of multiple 4mmx4mm dies dropped on a larger pattern (20mmx20mm) of adhesive s(a) optical camera, (b) X-Ray scan showing no large voids at the centre.

Os), void formation is expected to be minimal.

5.2. Die-shear strength

Die-shear strength measurements were carried out at room temperature using a Nordson DAGE 4000 Bondtester for the 1 mm × 1 mm dies (instrument limit: 50 N) and a Royce 650 Universal Bond Tester for the larger die sizes. In all cases, the tests were performed, with the die-shear tool positioned 100 μm above the substrate and operated at a constant shear speed of 200 μm/s [32].

Mounting pressure was found to have a pronounced effect on die shear strength. For each die size, the adhesive volume was kept constant regardless of the attachment method. Under these conditions, dies attached without mounting pressure exhibited significantly lower shear strength than those attached with pressure. Nevertheless, the measured low shear strength values remained within the specification provided by the adhesive material's technical data sheet (TDS) (9.62 MPa). In contrast, the application of mounting pressure resulted in shear strength values that substantially exceeded the TDS reference value. Fig. 22 shows the average die shear strength for the investigated die sizes and surface conditions.

A preliminary explanation for this discrepancy is the excess deposition of adhesive, which, under applied pressure, led to the formation of a large adhesive fillet that directly enhanced the bond strength. To validate this assumption, a reduced adhesive volume was printed using a smaller stencil aperture relative to the pad size, specifically, stencil aperture of 2.2 mm × 2.2 mm were used to print adhesive at the centre of 3.25 mm × 3.35 mm pads, while stencil aperture of 3.25 mm × 3.25 mm were applied at the centre of 4.3 mm × 4.3 mm pads, and then dies were attached with 1 MPa of mounting pressure.

Post-assembly inspection of these samples confirmed minimal to no fillet formation. Subsequent testing revealed their shear strength was only marginally higher than that of the non-pressure baseline, indicating that the application of pressure itself had slight effect on bond strength compared to the presence of the adhesive fillet. Fig. 23 shows the average die shear strength of dies attached with applied pressure where no fillet was formed.

The experimental results showed no direct correlation between die shear strength and die size. Although a size effect might be expected, the data did not support such a trend [33]. A major confounding factor was the non-uniform bond line thickness (BLT) across the sample set. This variation arose from the manual stencil printing process, where the adhesive deposit thickness depended on the stencil aperture designed for each die size.

Adhesion is fundamentally a surface-dependent phenomenon, and the characteristics of the surfaces being joined play a critical role in determining the strength and long-term durability of the resulting bond. Metallic substrates are typically covered by oxide layers that originate during manufacturing or are generated during subsequent processing steps such as cleaning, machining, milling, or forming. Both the chemical composition and the morphological features of these surface layers significantly influence the bonding process and, consequently, the performance of the adhesive joint. Several theories have been proposed to explain adhesion mechanisms, all emphasizing the importance of surface properties in achieving successful bonding [34,35].

The weak boundary layer theory suggests that effective adhesion requires intimate contact between the interacting surfaces. Surface contaminants, including grease, dust, and particulate matter, can act as weak interfacial layers that prevent close contact and thereby reduce adhesion [34,35].

The diffusion theory is primarily applicable to polymeric materials. According to this mechanism, polymer chains from adjacent surfaces interpenetrate across the interface, forming a bond through molecular diffusion. This process resembles solvent welding and is generally not relevant for metal substrates. Furthermore, its contribution is limited in highly cross-linked or crystalline polymers due to restricted molecular mobility [34,35].

The electrostatic theory proposes that when two metallic surfaces are brought into very close proximity, electron transfer may occur, generating attractive electrostatic forces. While this mechanism can explain adhesion in certain metal-to-metal contacts, such as precision gauge blocks, it is not considered applicable to adhesive joints involving polymer-based adhesives because these materials do not support the formation of shared metallic electrons [34–36].

According to the mechanical interlocking theory, adhesion is achieved when a liquid adhesive penetrates surface irregularities, pores, or cavities and subsequently solidifies, creating a mechanical anchor within the substrate. This mechanism is particularly plausible for rough or porous materials, such as wood or metals with highly porous oxide layers. However, the improved adhesion often observed on roughened surfaces may also result from other factors, including increased surface area, removal of contaminants, and enhanced wetting behavior, rather than solely from mechanical interlocking [37,38].

The physical adsorption theory attributes adhesion to intermolecular forces that develop when the adhesive and adherend are brought into close contact. These interactions may involve primary valence forces or secondary forces, such as van der Waals interactions. Secondary forces, including dipole–dipole, dispersion, and hydrogen-bonding interactions, are widely regarded as the predominant contributors to adhesion at the interface. In particular, polar and dispersion forces are believed to provide significant attractive interactions because of their relatively longer interaction distances. Adhesion has also been interpreted through acid–base interactions, where one material acts as an electron donor and the other as an electron acceptor, leading to interfacial bonding [35,39].

The chemical bonding theory proposes that strong ionic, covalent, or metallic bonds can form directly across the adhesive–adherend interface. These bonds generally exhibit higher strength than secondary intermolecular forces but require much closer atomic contact due to

their shorter interaction distances. Metallic bonding is only possible when metallic materials are present on both sides of the interface and is therefore of limited relevance to most adhesive systems [34,35,39].

Current understanding suggests that adhesion is typically governed by a combination of mechanisms, with physical adsorption, chemical bonding, and mechanical interlocking often contributing simultaneously to bond formation [34,39]. The effectiveness of these mechanisms is generally enhanced by increased surface area. Consequently, an adhesive joint should be viewed as a multilayered interfacial system in which several adhesion mechanisms may operate concurrently.

The application of bonding pressure generally plays a secondary role in adhesive joint formation. Its primary and adherend surfaces, thereby improving wetting and reducing the presence of interfacial voids. In addition, moderate pressure can enhance the density and uniformity of the adhesive layer by facilitating the redistribution of the uncured material. However, the beneficial effect of pressure is limited. Excessive bonding forces may cause adhesive squeeze-out, resulting in a reduced bond-line thickness and insufficient adhesive coverage of the bonding area. Consequently, beyond an optimum range, increasing the applied pressure can negatively affect joint integrity and lead to a reduction in bond strength.

In general, the joining of materials can be achieved by connecting two parts using an adhesive, where the resulting bonding forces hold the components together. The adhesive joint interface typically involves several bonding mechanisms, including mechanical interlocking, chemical bonding, diffusion, and electrostatic attraction [40,41]. The die-shear strength is usually the combined effect of all these forces.

Fig. 20 shows the main adhesive bonding mechanisms.

The AFM scan shown in Fig. 21 reveals a fine polycrystalline grain structure with clearly defined grain boundaries and nanoscale height variations. The film exhibits low RMS surface roughness, consistent with controlled thin-film fabrication.

5.3. Failure analysis

Following the die-shear tests of the original assembly where adhesive fillet was present, as well as the assemblies produced without mounting pressure, a comprehensive failure analysis was conducted on both the PCB pad side and the die side to determine the failure mode and characterize the fracture surfaces. The analysis employed a 3D laser scanning microscope for topographical imaging and a desktop SEM equipped with (EDS) for elemental composition analysis. Initial optical inspection revealed the presence of residual adhesive on both the die surface and the PCB pads across all surface finishes and assembly conditions, indicative of mainly a cohesive failure mechanism. Subsequent high-resolution 3D profilometry (Figs. 24 and 25) and EDS mapping (Figs. 26 and 27) confirmed these findings, verifying the consistent presence of adhesive material on both fracture surfaces. Fig. 23 shows an illustration for the various failure modes associated with die-shear testing (see Fig. 28).

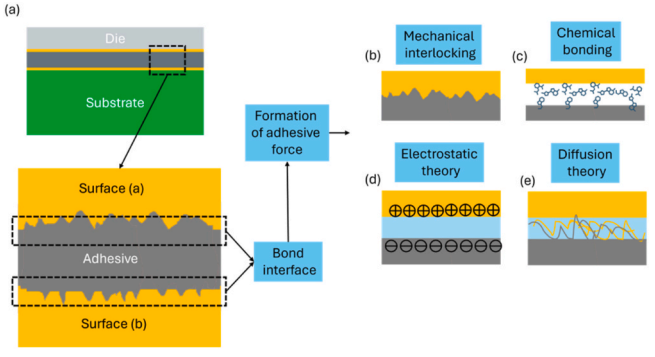


Fig. 20. Adhesive bonding mechanism (a) bond interface, (b) mechanical interlocking, (c) chemical bonding, (d) electrostatic theory, (e) diffusion theory.

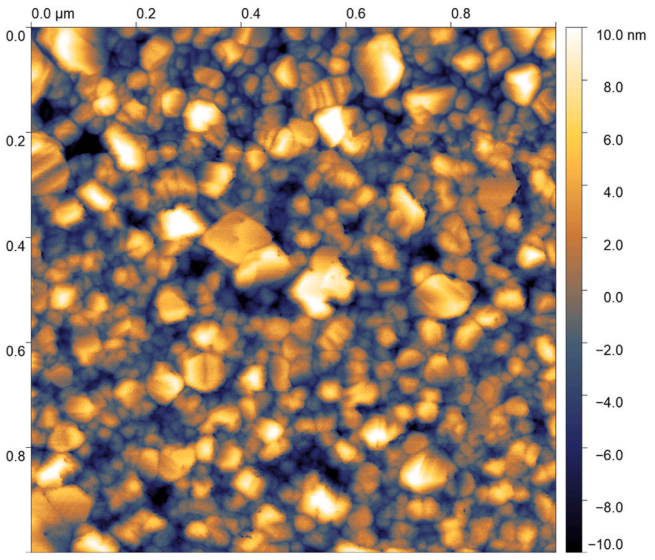


Fig. 21. Atomic Force Microscopy (AFM) topography map of a silver thin-film deposited through evaporation.

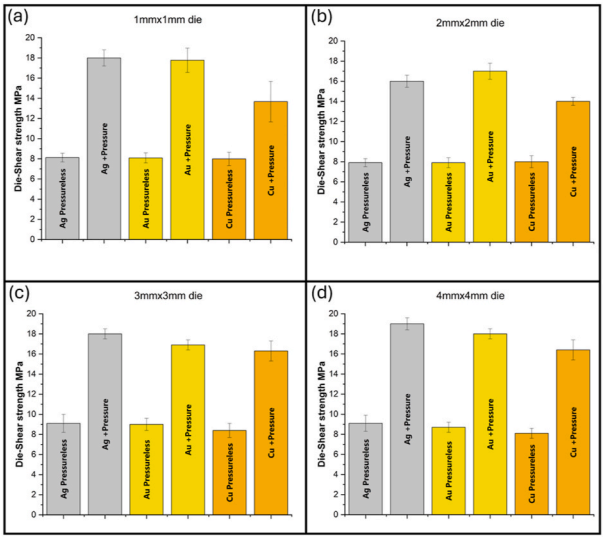


Fig. 22. Die-shear strength of different die sizes and surface finishes assembled with and without mounting pressure (a) 1mmx1mm, (b) 2mmx2mm, (c) 3mmx3mm, (d) 4mmx4mm.

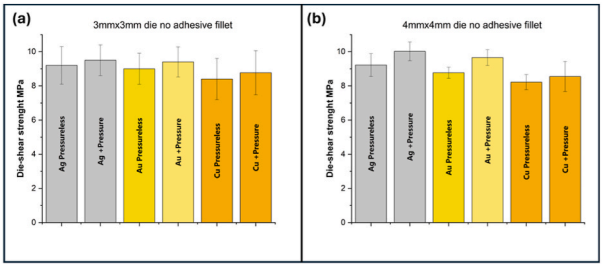


Fig. 23. Die-shear strength of different die sizes and surface finishes with and without mounting pressure (a) 3mmx3mm, (b) 4mmx4mm, where the adhesive volume was optimized to minimize the adhesive fillet formation.

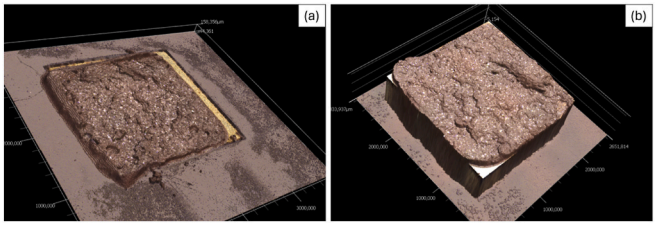


Fig. 24. 3D surface scans of samples assembled using the drop-attach method after die-shear testing, showing adhesive residues on (a) the PCB pad surface and (b) the die surface(Ag).

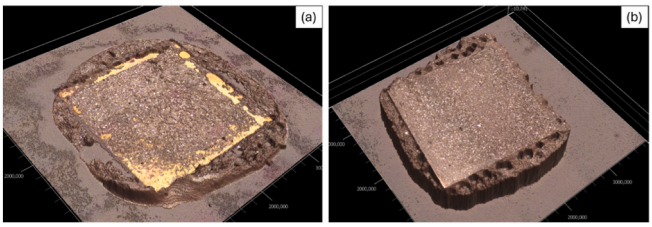


Fig. 25. 3D surface scans of samples assembled using pick-and-place after die-shear testing, showing adhesive residues on (a) the PCB pad surface and (b) the die surface(Ag).

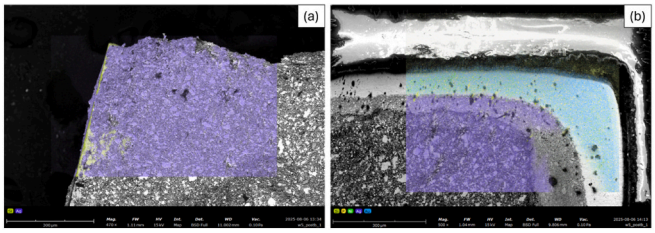


Fig. 26. SEM/EDS mapping of samples assembled using the drop-attach method after die-shear testing, confirming the presence of silver adhesive residues on (a) the die surface and (b) the PCB pad surface.

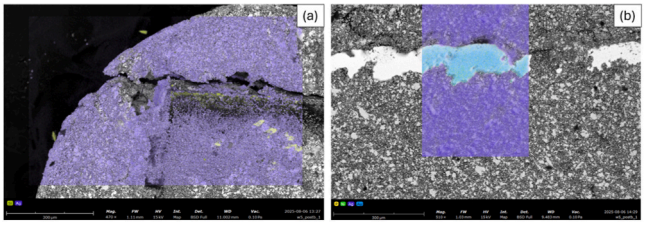


Fig. 27. SEM/EDS mapping of samples assembled using pick-and-place after die-shear testing, confirming the presence of silver adhesive residues on (a) the die surface and (b) the PCB pad surface.

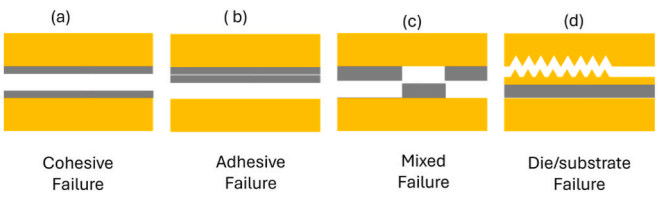


Fig. 28. Failure modes, (a) Cohesive, (b) Adhesive, (c) Mixed, and (d) Die/substrate failure.

5.4. Bond interface microstructure

To examine the bond interfaces, samples were first mounted using KEM 20 cold mounting resin, followed by grinding and polishing with a Qpol 300 M2 machine. Microstructural examination and elemental analysis were performed using SEM and EDS. No significant differences were observed at the bond interfaces across the different surface finishes. However, a notable feature was observed which is the formation of an adhesive fillet at the bond interface, caused by excess material being displaced under the applied bond force. As illustrated in Fig. 29 (a), the adhesive fillet is clearly visible, in contrast to the absence of fillet in Fig. 29(b). In addition, the adhesive layer was consistently thinner in dies attached using the pick-and-place method compared with those attached via the drop-attach method which is in agreement with the BLT values obtained from the 3D-scans. Fig. 30 show an example of the bond interface where (a) for die attached with pressure application and (b) for a die attached with the drop-attach method.

As discussed in Section(A) X-ray inspection, several large defects were detected at the centre of the dies attached with no pressure. To validate their nature and origin, the bond interface at the defect sites was further examined using SEM. Fig. 31(a) shows delamination of the adhesive from the die surface suggesting poor adhesion, while Fig. 31(b) reveals voids within the printed profile. These voids are likely caused by non-uniform volume shrinkage of the adhesive during curing, which results in discontinuities within the printed adhesive film. Another factor which can lead to such defects is the grinding and polishing process to prepare the specimen, to clarify the reason, several samples were inspected and showed that such defects are only detected and the void site detected by X-ray imaging.

5.5. Electrical characterization

The sheet resistance of the dummy wafers was measured using CDE ResMAP 178 and the effective resistivity of the dies surfaces was calculated accordingly. The values obtained were $2.86 \times 10^{-8}\Omega.m$ for Au, $3.04 \times 10^{-8}\Omega.m$ for Cu and $2.74 \times 10^{-8}\Omega.m$ for Ag. The ENIG finished pads effective resistivity was calculated to be $2.94 \times 10^{-5}\Omega.m$.

PCBs with electrical test structures were used to evaluate the electrical performance of the die attachment methods. The design contained simple structures of daisy chain (DC). The DC structure allowed the bridging of six 1 mm-by-1 mm dummy dies. Fig. 32 shows the PCB design used for the test.

To mitigate issues arising from material spread under applied mounting pressure—specifically, the risk of short circuits across the narrow gaps between adjacent PCB electrodes—the adhesive paste deposition methodology was adapted accordingly. For dies mounted under pressure, the conductive adhesive was not printed via stencil printing but was instead manually dispensed as three discrete dots along each electrode so that the volume deposited is around 50% less in comparison with the stencil printed volume. This approach successfully contained the material flow during compression, and post-assembly

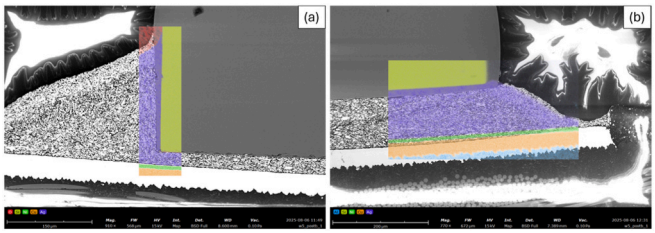


Fig. 29. SEM/EDS mapping of the bond interface between dies and a PCB: (a) Die attached using the pick-and-place method, showing the formation of an adhesive fillet around the bond line; (b) Die attached via the drop-attach method, where no adhesive fillet is observed.

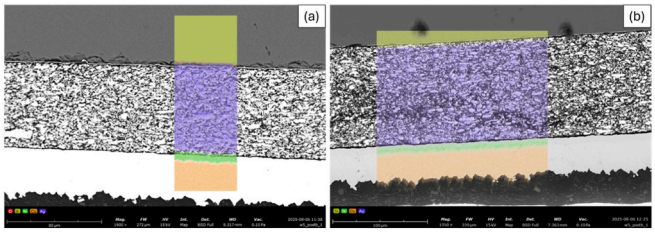


Fig. 30. SEM/EDS mapping of the bond interface between dies and a PCB: (a) Die attached using the pick-and-place method, (b) Die attached via the drop-attach method.

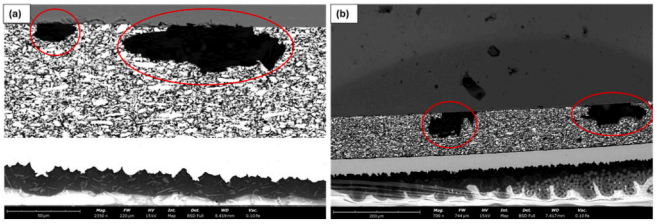


Fig. 31. SEM scan at the defect regions observed by the X-Rays (a) showing delamination of adhesive film (b) shows discontinuity of the printed adhesive film.

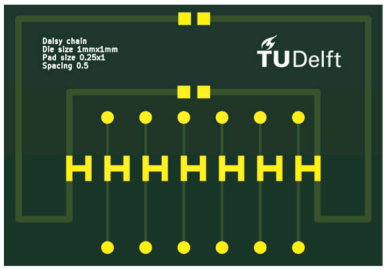


Fig. 32. PCB design with daisy chain structures.

inspection confirmed the absence of short circuits. For dies attached without pressure, the adhesive was printed using a standard 100 μm thick stencil, as there was no risk for short circuits.

The electrical measurements were performed using Summit 11K/12K Probe Station. Resistance measurements across the DC test structures demonstrate that the application of mounting pressure plays a decisive role in determining the electrical performance of the assemblies. Samples assembled under pressure exhibited consistently lower resistance values compared to their pressure-less counterparts.

The highest chain resistance was observed for Cu dies attached using the drop-attach method, whereas the lowest values were obtained for Ag dies attached by conventional pick-and-place. For dies assembled without applied pressure, the overall chain resistance increased by 21.92% to 42.41%, underscoring the critical influence of pressure application on the adhesive performance. Fig. 33 shows the measured total chain resistance for all dies and conditions where the BLT varied significantly.

The elevated resistance in pressure-less assemblies can be attributed to insufficient particle bridging and incomplete formation of conductive networks, both of which limit current transport and thereby degrade the electrical reliability of the interconnects. However as the BLT varied significantly between dies attached with and without pressure, this higher resistance couldn't be fully explained. For that reason several tries have been made to ensure similar BLT, despite the challenges and the failures, the only solution which was to some extent successful is using a thinner stencil of only 50μm instead of the 100μm used for the

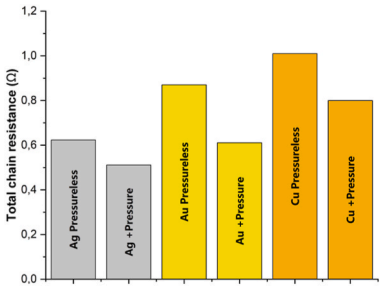


Fig. 33. Total resistance measured across the DC for different 1mmx1mm dies attached with and without pressure with a varying BLT.

previous experiments. By employing this stencil the BLT of the dies attached without pressure was matching the BLT of the dies attached with pressure as described earlier. Due the manual printing method this method wasn't reproducible enough so only Ag and Au dies were tested.

Upon resistance measurements of the dies attached without pressure a significant reduction in resistance was observed compared to the previous set of dies. Overall the resistance of the dies attached with pressure with a similar BLT showed a maximum increase of 9.55% compared to the previous measured increase of 42.41%. This validate the BLT and the amount of the adhesive had a great influence on the resistance of the circuit. Despite the improve of the resistance values measured it was still higher than those attached with applied pressure. While these results confirm that insufficient particle bridging and incomplete conductive network formation contribute to the resistance, their impact appears less significant compared to the initial observation. The limited influence can be attributed to the high metal contact >80%, which ensured a conductive path even without pressure application. Fig. 34 shows the total chain resistance of silver and gold surface finish dies and conditions where the BLT were matched.

As discussed in the initial trials, the current setup using a manual stencil printer was not capable of producing the fine printed structures required for reliable electrical characterization. To address these limitations, an automatic stencil printer (DEK TQ-ASMPT) was used together with a PCB containing daisy chain test structures.

Two printing strategies were investigated. In the first scenario, the entire pad area was covered with adhesive material. During pressure application, the adhesive spread beyond the intended region, leading to electrical short circuits between adjacent structures. In the second scenario, a smaller adhesive pattern was printed at the centre of the pad to reduce excessive spreading. Nevertheless, this resulted in non-uniform material distribution beneath the die. Since both the pad geometry and the printed pattern were rectangular, the adhesive did not spread evenly across the interface, causing inconsistent coverage and unreliable

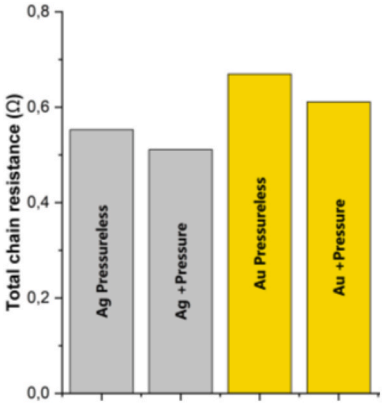


Fig. 34. Total resistance measured across the DC for different 1mmx1mm dies attached with and without pressure with a constant BLT.

contact formation. Fig. 35 shows illustrations of the two strategies considered for adhesive printing.

As a result, neither printing strategy provided sufficiently reliable structures for electrical characterization, and therefore these approaches were not pursued further in this study.

An alternative approach was subsequently investigated using the dispensing unit of the automatic dispensing system. Since the original design was intended for 1 mm × 1 mm dies, the DC pads were relatively small. Due to the dispensing resolution limitations, it was therefore not possible to print commonly used adhesive patterns, such as cross, double-cross, or asterisk shapes, on the pads. Consequently, a modified design was fabricated to enable bridging between three 3 mm × 3 mm dies.

In this method, a thin adhesive layer with a thickness of approximately 20 μm was precisely deposited onto the PCB pads. Based on an analysis of the dispensing system parameters, an equivalent adhesive volume was dispensed in the form of a special pattern for the rectangle form [42].

Fig. 36 shows an illustration of the adhesive print pattern.

During the die attach process, the applied pressure caused the printed pattern to spread beneath the die, promoting full interface coverage.

Nevertheless, achieving complete coverage without the formation of a minimal adhesive fillet was not feasible. The fillet volume was estimated to exceed 10% of the total dispensed adhesive volume. Therefore, for dies attached under pressure, the dispensed adhesive volume was increased by approximately 10% to compensate for the material loss associated with fillet formation. Fig. 37 shows an X-ray image of 3mmx3mm dies attached on PCB with daisy chain structure.

Upon successful assembly, the total chain resistance of each PCB was measured. The results are presented in Fig. 38. A slight reduction in resistance was observed across all PCBs compared to the initial measurements. This decrease is primarily attributed to the larger die area, which provides an increased contact interface. However, the most notable observation is that assemblies produced without pressure application consistently exhibited a slightly higher resistance. These results indicate that pressure application has a positive effect on the overall electrical conductivity of the assembly. Nevertheless, the die surface metallurgy appears to have a more pronounced influence on conductivity than the assembly method.

The total chain resistance was strongly influenced by both the metallization material and the application of pressure during assembly. Applying pressure reduced the resistance by approximately 13% for Ag-based samples, 12% for Au-based samples, and 4% for Cu-based samples. Among the tested metallizations, Ag exhibited the lowest resistance, while Au and Cu showed increases of approximately 43% and 66%, respectively, under pressure less conditions relative to Ag. A similar trend was observed under pressure-assisted conditions, where the resistance of Au and Cu remained approximately 44% and 82% higher than that of Ag. Overall, pressure improved the electrical performance for all metallizations, with the most pronounced effect observed for Ag and Au.

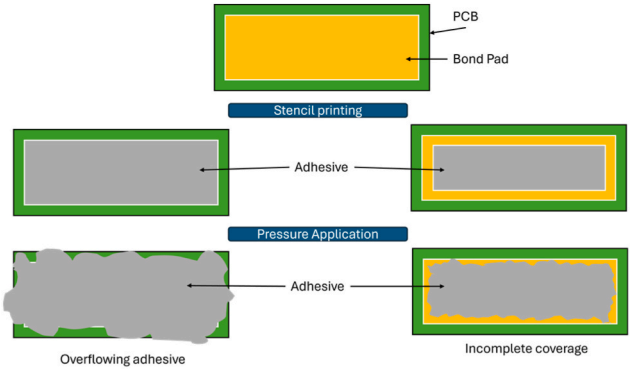


Fig. 35. Illustration for the two scenarios tested using the automatic stencil printer.

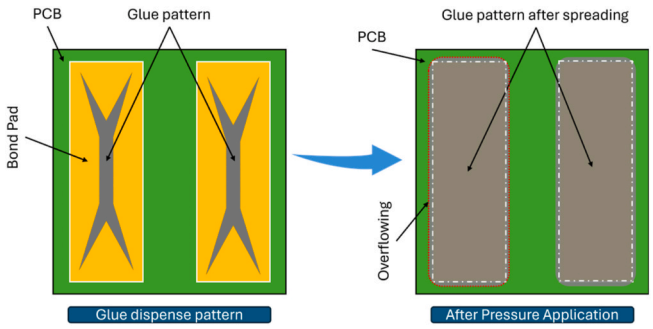


Fig. 36. Glue pattern used for coating the daisy chain pads for dies attached with pressure.

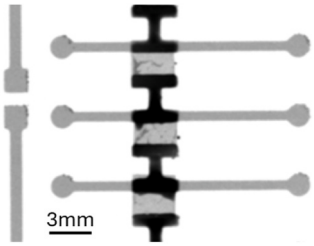


Fig. 37. X-ray image of a PCB with daisy chain structures attached with applied pressure.

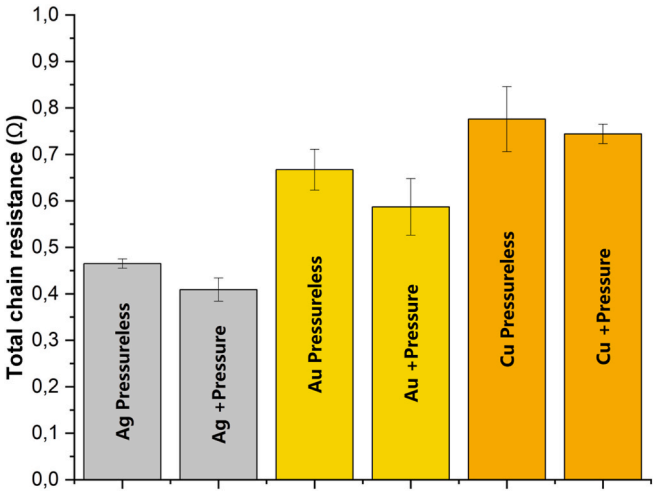


Fig. 38. Total chain resistance measured across the DC for different 3mmx3mm dies attached with and without pressure.

6. Conclusion

In this study, dies with Ag, Cu, and Au surface finishes were attached using both the conventional pick-and-place method and a proposed drop-attach approach that eliminates the requirement for mounting pressure.

The results demonstrate the feasibility of contact-less die attachment method using adhesive and highlight its potential for applications involving delicate or pressure-sensitive components, while also offering a significant increase in throughput for industrial-scale assembly processes.

A key requirement for successful pressure-less die bonding is the presence of a uniform, flat adhesive layer with minimal imperfections. Such layers can be produced using stencil printing technology or more advanced approaches such as laser-induced forward transfer (LIFT), whereas conventional dispensing techniques may not adequately meet these requirements.

The most pronounced difference between the two approaches is the bond line thickness (BLT) at a constant adhesive volume, which was consistently higher for drop-attach. To comply with industry specifications for BLT, the dispensing process must therefore be optimized, either by employing thinner stencils to reduce the deposited volume or by applying Laser-Induced Forward Transfer (LIFT) for highly controlled patterning of adhesive.

In addition, the presence of an adhesive fillet was found to enhance mechanical reliability, with conventional attachment achieving approximately 45% higher die-shear strength relative to drop-attach when the same adhesive volume is used.

Testing the samples attached with pressure, where no adhesive fillet was formed, the dies-shear strength was limited to maximum of 12.7% higher when compared to samples attached with no pressure. This demonstrates that while pressure application can enhance bond strength, the improvement is relatively modest. In contrast, the presence of an adhesive fillet plays a more significant role in reinforcing the joint and improving its mechanical reliability. in other words, applying pressure does not significantly improve wetting because the thin films already exhibit minimal surface roughness. This low surface roughness results from the thin-film deposition technologies used to fabricate the surfaces, which inherently produce highly uniform and smooth layers allowing the adhesive to wet the surfaces without the need for pressure application.

Electrical performance was to some extent negatively affected, as the absence of pressure led to an increase in total chain resistance, independent of surface metallization. Nonetheless, the magnitude of this resistance increase was influenced by the die surface metallization, indicating that the compatibility of the bonded surfaces is a key parameter for the successful implementation of this die attach method. Our experiments showed the significant influence of the BLT and adhesive volume on the electrical resistance of the assembly, nevertheless dedicated experiments should be considered for future work to assess the contact resistivity and long term reliability.

It was observed that the absence of applied pressure during die mounting resulted in defects, predominantly in the form of voids. Several factors may contribute to the formation of these defects, warranting further investigation and the development of strategies for their mitigation. Nonetheless, the void fraction remains below the maximum threshold of 25% specified by the IPC standard for electronic assembly acceptance. As this standard primarily pertains to solder joints, additional studies are required before the applicability of the pressure-less mounting method can be recommended for specific applications.

One possible explanation lies in the fundamental difference between the conventional and pressure-less assembly processes. In the conventional process, the die is brought into contact with the adhesive and subsequently pressed into it. This squeezing action promotes adhesive flow and facilitates the evacuation of trapped air from the die–adhesive interface, thereby reducing the likelihood of void formation. In contrast, during pressure-less assembly, the die is released onto the adhesive without the application of an external force. In the ideal case, the die is released parallel to the substrate and lands on a flat, uniform adhesive surface. Upon contact, the adhesive rapidly wets and seals the die–adhesive interface, which may restrict the escape of air trapped beneath the die and increase the likelihood of void formation. In addition, some voids may originate from volatile compounds or entrapped gases within the adhesive formulation itself, which can be released during curing irrespective of the attachment method. Therefore, the observed void content is likely the result of a combination of air entrapment during die placement and gas evolution from the adhesive during the curing process.

Unlike conventional pick-and-place, which requires controlled deceleration over the final ~100 μm landing distance (adding 5–10 ms per cycle), drop-attach permits high-speed motion until the die is approximately 100–300 μm above the substrate, at which point release occurs. This substantially reduces cycle time and, when implemented on industrial-scale automatic die bonders, has the potential to significantly increase process throughput. Importantly, it does not require any redesign of existing equipment but can be implemented by adjusting current tool settings.

These trade-offs must be considered when defining appropriate use cases. Nevertheless, drop-attach provides significant advantages for pressure-sensitive and fragile dies and enables much shorter assembly times. While the present study demonstrates the feasibility of the proposed process, long-term reliability evaluations remain necessary to determine its robustness under operating conditions.

A particularly relevant application of this method is micro-LED assembly, where millions of dies must be placed with high accuracy. In such high-volume manufacturing, the cumulative deceleration steps required by conventional pick-and-place make the process extremely time-consuming. Drop-attach, by contrast, offers a pathway to drastically improve assembly efficiency. Although the technique may introduce certain performance trade-offs—such as constraints on the achievable electrical or mechanical properties of the final interconnect—it still enables high-speed operation with performance levels acceptable for large-scale micro-LED production. These trade-offs can be mitigated by employing high-performance materials with enhanced electrical conductivity and mechanical strength, helping ensure that the final bond quality remains within industry-accepted limits.

7. Future work

This study represents an initial step toward understanding bond quality and evaluating the feasibility of die attachment without the use of mounting pressure. Our findings indicate that a pressure-free process can increase die-attach efficiency by reducing cycle times and offers clear advantages for high-throughput assembly. However, several trade-offs limit its suitability for more demanding applications such as power devices.

An additional challenge is the alignment accuracy of die placement when dies are released from a distance above the substrate. This aspect is not addressed in the present study, as a reliable assessment of alignment first requires eliminating other potential sources of variation—such as differences in pad dimensions and orientation from the PCB manufacturer, as well as inconsistencies introduced during adhesive printing.

Declaration of competing interest

The authors declare the following financial interests/personal relationships which may be considered as potential competing interests: Ahmed Abdelwahab reports financial support was provided by Netherlands Enterprise Agency (RVO). Ahmed Abdelwahab reports financial support was provided by ITEC B.V. Ahmed Abdelwahab has patent #PCT/EP2024/070643, A METHOD FOR MOUNTING AN ELE CTRONICS COMPONENT AT A PAR TICULAR PLACEMENT LOCATION O N A CARRIER AS WELL AS A PICK-A ND-PLACE APPARATUS FOR MOUN TING AN ELECTRONICS COMPONE NT AT A PARTICULAR PLACEMENT LOCATION ON A CARRIER. pending to NEXPERIA B.V. If there are other authors, they declare that they have no known competing financial interests or personal relationships that could have appeared to influence the work reported in this paper.

Acknowledgement

This work was funded by ITEC B.V. and co-financed by the

Netherlands Enterprise Agency (RVO). The authors would like to thank the Else Kooi Laboratory (EKL), Kavli Nanolab Delft, and the Chip Integration Technology Centre (CITC) for their valuable support and contributions to this research, and Herman Ten Berge from Acal BFi and his company for providing the high-speed camera footage.

Appendix A. Supplementary data

Supplementary data to this article can be found online at https://doi.org/10.1016/j.jmrt.2026.06.226.

References

[1] Nassiet V, Hassoune-Rhabbour B, Tramis O, Petit J-A. 22 - electrical and electronics. In: Adams RD, editor. Adhesive bonding. second ed. Woodhead Publishing; 2021. p. 719–61.
[2] Zhang H, Suganuma K. Sintered silver for LED applications. In: Siow KS, editor. Die-Attach materials for high temperature applications in microelectronics packaging: materials, processes, equipment, and reliability. Cham: Springer International Publishing; 2019. p. 35–65.
[3] Maxfield C, Waddell P. Chapter 21 - alternative and future technologies. In: Maxfield C, Waddell P, editors. Bebop to the boolean boogie. second ed. Burlington: Newnes; 2003. p. 290–340.
[4] Riegger L, Strohmeier O, Faltin B, Zengerle R, Koltay P. Adhesive bonding of microfluidic chips: influence of process parameters. J Micromech Microeng 2010; 20(8):087003. https://doi.org/10.1088/0960-1317/20/8/087003. 2010/07/12.
[5] Su Y, Zhang L, Liao B, Mai YL, Dai YQ, Hu W. Simultaneous improvement of the electrical conductivity and mechanical properties via double-bond introduction in the electrically conductive adhesives. J Mater Sci Mater Electron 2020;31(11): 8923–32. https://doi.org/10.1007/s10854-020-03427-2. 2020/06/01.
[6] Yim MJ, Yi L, Kyoung-sik M, Wook PK, Wong CP. Review of recent advances in electrically conductive adhesive materials and technologies in electronic packaging. J Adhes Sci Technol 2008;22(14):1593–630. https://doi.org/10.1163/156856108X320519. 2008/01/01.
[7] Zhang W, et al. Electrical and mechanical reliability and failure mechanism analysis of electrically conductive adhesives. Microelectron Reliab 2023;151: 115236. https://doi.org/10.1016/j.microrel.2023.115236. 2023/12/01/.
[8] Xiao G, et al. Mechanical properties of cured isotropic conductive adhesive (ICA) under hygrothermal aging investigated by micro-indentation. Int J Solid Struct 2017;122–123:81–90. https://doi.org/10.1016/j.ijsolstr.2017.06.003. 2017/09/01/.
[9] Zhang XM, Yang X-L, Wang B. Electrical properties of electrically conductive adhesives from epoxy and silver-coated copper powders after sintering and thermal aging. Int J Adhesion Adhes 2021;105:102785. https://doi.org/10.1016/j.ijadhadh.2020.102785. 2021/03/01/.
[10] Nexperia BV. A method for mounting an electronics component at a particular placement location on a carrier as well as a pick-and-place apparatus for mounting an electronics component at a particular placement location on a carrier. 2024.
[11] Bertin CL, Su L-S, Van Horn J. Known Good Die (KGD). In: Puttlitz KJ, Totta PA, editors. Area array interconnection handbook. Boston, MA: Springer US; 2001. p. 149–200.
[12] Majeed B, Paul I, Razeeb KM, Barton J, O'Mathuna SC. Microstructural, mechanical, fractural and electrical characterization of thinned and singulated silicon test die. J Micromech Microeng 2006;16(8):1519. https://doi.org/10.1088/0960-1317/16/8/012. 2006/06/22.
[13] Talledo J. Investigation on Die Crack in a Stacked Die Package Using Finite Element Analysis. J Eng Res Rep 2021;20(3):83–91. https://doi.org/10.9734/jerr/2021/v20i317285.
[14] Zirilli T. Die crack failure mechanism investigations depending on the time of failure. Microelectron Reliab 2015;55(9):1600–6. https://doi.org/10.1016/j.microrel.2015.06.148. 2015/08/01/.
[15] Zaal JJM, van Driel WD, van Beek JTM, Zhang GQ. In: Ernst LJn, Zhang GQn, Driel WDv n, Rodgers Pn, Bailey Cn, Saint Leger Od n, editors. Assembly induced failures in thin film MEMS packages. IEEE; 2009. p. 227–31.
[16] Zaal JJ, van Driel WD, Zhang GQ. Challenges in the assembly and handling of thin film capped MEMS devices. Sensors 2010;10(4):3989–4001. https://doi.org/10.3390/s100403989 (in eng).
[17] Ma L, Bao SX. Failure Analysis of Cracked Die. ECS Trans 2010;27(1):281. https://doi.org/10.1149/1.3360633. 2010/11/23.
[18] Ranjan M, Gopalakrishnan L, Srihari K, Woychik C. Die cracking in flip chip assemblies. In: 1998 proceedings. 48th electronic components and technology conference (Cat. No.98CH36206); 1998. p. 729–33. https://doi.org/10.1109/ECTC.1998.678779. 25-28 May 1998.
[19] Abdelwahab A, Zeijl HV, Hoorn RV, Kuipers H, Mastrangeli M. Pick-and-Release: a Novel Contactless Bonding Method for Die Attachment. In: 2025 IEEE 75th electronic components and technology conference (ECTC); 2025. p. 2125–32. https://doi.org/10.1109/ECTC51687.2025.00363. 27-30 May 2025.
[20] Myśliwiec M, Kisiel R. Die attachment Process Overview for High Power Semiconductors. 2023 46th international Spring seminar on electronics technology (ISSE). 2023. p. 1–5.
[21] Alim MA, Abdullah MZ, Aziz MSA, Kamarudin R. Die attachment, wire bonding, and encapsulation process in LED packaging: a review. Sensor Actuator Phys 2021; 329:112817. https://doi.org/10.1016/j.sna.2021.112817. 2021/10/01/.
[22] Kim J, Zhang Z, Won D, Yoon SW, Jin Y. A pick-and-place process control based on the bootstrapping method for quality enhancement in surface mount technology. Int J Adv Manuf Technol 2024.
[23] Kim B-K, et al. Origin of surface defects in PCB final finishes by the electroless nickel immersion gold process. J Electron Mater 2008;37(4):527–34. https://doi.org/10.1007/s11664-007-0360-9. 2008/04/01.
[24] Shen C, et al. Packaging reliability effect of ENIG and ENEPIG surface finishes in board level thermal test under long-term aging and cycling. Materials Apr 26 2017; 10(5). https://doi.org/10.3390/ma10050451 (in eng).
[25] Wang MY, Mei YH, Burgos R, Boroyevich D, Lu GQ. Effect of substrate surface finish on bonding strength of pressure-less sintered silver die-attach. In: 2018 international conference on electronics packaging and iMAPS all Asia conference (ICEP-IAAC); 2018. p. 50–4. https://doi.org/10.23919/ICEP.2018.8374668. 17-21 April 2018.
[26] Bulíček M, Málek J, Rajagopal KR. On Kelvin-Voigt model and its generalizations. Evol Equ Control Theor 2012;1(1):17–42. https://doi.org/10.3934/eect.2012.1.17. 2012/03/01.
[27] Chen P-C, Ming C, Wei-Chung L, Gabayno JL. Bond line thickness and die tilt inspection in die bonding process. J Chin Inst Eng 2016;39(4):508–12. https://doi.org/10.1080/02533839.2015.1125795. 2016/05/18.
[28] Yavorsky BM, Pinsky AA. Fundamentals of physics: motion and forces. Conservation laws. Molecular-kinetic theory of gases. Molecular forces and states of aggregation of matter. Electrodynamics (no. v. 1). Mir; 1975.
[29] Moss EA, Krassnokutski A, Skews BW, Paton RT. Highly transient squeeze-film flows. J Fluid Mech 2011;671:384–98. https://doi.org/10.1017/S0022112010005756.
[30] Lang J, Nathan R, Wu Q. Experimental Study of transient squeezing film flow. J Fluid Eng 2019;141(8). https://doi.org/10.1115/1.4042758.
[31] Espìn L, Papageorgiou DT. Viscous pressure-driven flows and their stability in channels with vertically oscillating walls. Phys Fluids 2012;24(2). https://doi.org/10.1063/1.3690904.
[32] U. S. D. o. Defense. Test method standard: microcircuits (MIL-STD-883H). Washington, DC: Department of Defense; 2010. Military Standard 2010-02-26.
[33] Chen C, et al. Bonding technology based on solid porous Ag for large area chips. Scr Mater 2018;146:123–7. https://doi.org/10.1016/j.scriptamat.2017.11.035. 2018/03/15/.
[34] Adams RD, Comyn J, Wake WC. Structural adhesive joints in engineering. Netherlands: Springer; 1997.
[35] Groth M. Structural adhesive bonding of metals : surface and fracture mechanics aspects. PhD Thesis. 2001 [Online]. Available: https://www.researchgate.net/publication/35982989_Structural_adhesive_bonding_of_metals_surface_and_fracture_mechanics_aspects.
[36] Packham DE. Surface energy, surface topography and adhesion. Int J Adhesion Adhes 2003;23(6):437–48. https://doi.org/10.1016/S0143-7496(03)00068-X. 2003/01/01/.
[37] Kinloch AJ. Adhesives in engineering. Proc Inst Mech Eng G J Aerosp Eng 1997; 211(5):307–35. https://doi.org/10.1243/0954410971532703.
[38] Kinloch A. Adhesion and adhesives: science and technology. 1987.
[39] Petrie E. Handbook of Adhesives & Sealants. McGraw-Hill Education; 1999.
[40] Hu N, Shu L, Zheng X, Deng Z, Cang X. A review of modification methods, joints and self-healing methods of adhesive for aerospace. Sci Prog 2024;107(2): 00368504241242271. https://doi.org/10.1177/00368504241242271.
[41] Kweon J-H, Jung J-W, Kim T-H, Choi J-H, Kim D-H. Failure of carbon composite-to-aluminum joints with combined mechanical fastening and adhesive bonding. Compos Struct 2006;75(1):192–8. https://doi.org/10.1016/j.compstruct.2006.04.013. 2006/09/01/.
[42] Flaig F, Fräger T, Kaufmann M, Vallée T, Fricke H, Müller M. How to find the perfect application pattern for adhesively bonded joints? Journal of Advanced Joining Processes 2023;8:100147. https://doi.org/10.1016/j.jajp.2023.100147. 2023/11/01/.